Unconventional Aluminum Ion Intercalation/Deintercalation for Fast Switching and Highly Stable Electrochromism

*Yuyu Tian, Weikun Zhang, Shan Cong, Yuanchuan Zheng, Fengxia Geng, and Zhigang Zhao**

Electrochromic devices have many important commercial applications ranging from electronic paper like displays, antiglare rear-view mirrors in cars, to energy-saving smart windows in buildings. Monovalent ions such as H^+, Li^+, and Na^+ are widely used as insertion ions in electrochromic devices but have serious limitations such as instability, high-cost, and hard handling. The utilization of trivalent ions as insertion ions has been largely overlooked probably because of the strong electrostatic interactions between ions and intercalation framework and the resulted difficulties of intercalation. It is demonstrated that the trivalent ion, Al^{3+}, can be used as efficient insertion ion by using metal oxide hosts in nanostructured form, which brings the desired fast-switch, high-contrast, and high-stability as well to electrochromic devices. Differing from the usual structure degradation by repeated guest intercalation/deintercalation, the Al^{3+} insertion introduces strong electrostatic forces, which on some degree stabilize the crystal structure and consequently yield much enhanced performances.

1. Introduction

Electrochromism is a process involving controllable color change through electrochemical reactions, which is interesting from perspectives of both basic science and technology. It has found important applications ranging from electronic paper like displays, antiglare rear-view mirrors in cars, to energy-saving smart windows in buildings.[1–4] Transition metal oxides represent the most typical inorganic electrochromic material, the operation of which is based on reversible intercalation or deintercalation of ions into the lattice accompanied with valence change of metal ions.[5] The employed ions have so far been restricted to the monovalent ions, such as H^+, Li^+, and Na^+, probably due to the traditional concept that only monovalent ions would be easily incorporated into or released from the electrochromic material lattice,[6,7] for which, however, many drawbacks are present. When utilizing H^+ as the insertion ion, the cycle life of electrochromic devices has been generally degraded because acidic H^+ has a strong tendency to corrode surface of metal oxide electrode and additionally H^+ is easily polarized to form H_2 gas bubbles due to its low electrode potential.[8] While replacing acid with lithium (Li^+) salts-based electrolyte can bring enhanced electrochromic stability, a slower electrochromic response time (>10 s) is mostly an unavoidable cost.[9,10] Meantime, the handling of lithium-based electrochromic devices requires strict rules on environmental conditions because the salts are normally toxic and react strongly with air/moisture, in addition to the high-cost and limited lithium reserves in the earth's crust, which constitutes a big obstacle towards the development of lithium-based electrochromic devices.[11,12] Na^+-based device responses even slower due to the larger radius dimensions of Na^+ compared with that for H^+ or Li^+.[13] Therefore, it would be of particular importance to search for alternative cheap, stable, and rapid insertion ions in electrochromic devices to achieve cost-effective and rapid electrochromic application.

Numerous efforts have been taken to achieve the goal from the perspective of designing novel structures or adding dopants, with device performance improved to a certain extent while leaving the intrinsic problems concerning electrolyte optimization remained.[14–17] Although the utilization of multivalent ions as insertion ions has been largely overlooked, multivalent ions are expected to deliver enhanced coloration contrast due to the reason that the number of electrons injected into the framework per multivalent metal ion multiplies that for Li^+ or any other monovalent ions. The lack of

Y. Y. Tian, W. K. Zhang, Dr. S. Cong, Prof. Z. G. Zhao
Key Laboratory of Nanodevices and Applications
Suzhou Institute of Nanotech and Nanobionics
Chinese Academy of Sciences
398 Ruoshui Road, Suzhou Industry Park
Suzhou 215123, China
E-mail: zgzhao2011@sinano.ac.cn
Y. Y. Tian
Nano Science and Technology Institute
University of Science and Technology of China
166 Renai Road, Suzhou Industry Park
Suzhou 215123, China
Y. Zheng, Prof. F. X. Geng
College of Chemistry
Chemical Engineering and Materials Science
Soochow University
Suzhou 215123, China

DOI: 10.1002/adfm.201502638

studies probably results from the known great difficulties for the multivalent ions to intercalate because of the strong electrostatic interactions between the ions and the intercalation framework. The ever increasing development of nanotechnology has spawned a great innovative impact on various technological sectors, which may also bring new opportunities to electrochromic field.[16,18,19] The host material in nanostructured forms possesses many advantages, for example, short ion diffusion length, highly porous surface, and good contact with the conductive substrate, which could facilitate the insertion of guest ions. In this work, employing the most commonly used in organic electrochromic material,[20–22] tungsten oxide in nanowire morphology as an example, we illustrate that the trivalent ion, Al^{3+}, as insertion ion can bring the desired fast-switch, high-contrast, and high-stability as well to electrochromic devices. Al^{3+} was adopted because it has advantages of low-cost, environment friendly, and of most importance, small ionic radius. The findings are important for the basic research of electrochromism filed and open a new direction for achieving the long-desired stable, durable, and fast-switching electrochromic devices.

2. Results and Discussion

2.1. Sample Characterizations

A form of tungsten oxide nanomaterial, $W_{18}O_{49}$ nanowires, was employed as electrochromic host material in the present study, because $W_{18}O_{49}$ nanowires could display a reversible color change upon inserting or extracting ions induced by applying external voltage, appearing blue in the colored state or colorless in bleached state.[23,24] The electrochromic $W_{18}O_{49}$ nanowires were recently used as components in the design of a smart supercapacitor, which functions as a normal supercapacitor in energy storage and also communicates the level of stored energy through multiple-stage pattern indications.[24,25] Briefly, the $W_{18}O_{49}$ nanowires were grown on a fluorine-doped tin oxide (FTO)-coated glass substrate by solvothermal reaction of WCl_6 in ethanol solution at 180 °C for 12 h and subsequent annealing at 200 °C in argon atmosphere to achieve close contact at the interface. The phase identification and purity was characterized by X-ray diffraction (XRD), shown in **Figure 1**a, for which the material was scrapped off the substrate to avoid the interference from reflected signals of FTO on substrate. All the diffraction peaks could be clearly indexed as monoclinic $W_{18}O_{49}$ (*P*2/*m*, JCPDS no. 84-1516). The (010) reflections exhibited obvious narrowing and showed relatively high intensities, suggesting that the crystals preferably grew along the *b*-axis as a result of retarded growth along the close-packed (010) planes. $W_{18}O_{49}$ has a distorted ReO_3 structure in which corner-sharing distorted and tilt WO_6 octahedra are connected in the *a*-, *b*-, and *c*-directions,[26] with the projection view along the *b*-axis illustrated in the inset. The sample morphology was examined by scanning electron microscopy (SEM) characterizations (Figure 1b), which revealed that the sample was in nanowire morphology with average diameter of 10–20 nm and length of several micrometers. The inset depicts the high-resolution transmission electron microscopy (HRTEM) image of a single nanowire. Clear lattice fringes were observed, indicating that the nanowire was single-crystalline in nature. The fringes were perpendicular to the wire axis with spacing of 0.38 nm, corresponding to the (010) planes of monoclinic $W_{18}O_{49}$. This suggests that the nanowires were along the [010] direction, which is consistent with XRD results.

2.2. Electrochemical and Electrochromic Behavior in Aqueous Electrolyte

The electrochemical and electrochromic performance of the $W_{18}O_{49}$ nanowire film in aqueous electrolyte of trivalent ion, Al^{3+}, was following investigated, using $AlCl_3$ as an example. For comparison purpose, electrode performance in HCl and NaCl solutions was also studied. Electrolytes possessing the same anion were employed to exclude possible effects of anions. The electrode was switched repetitively 50 times with a 30 s polarity switching interval and electrochemical behaviors were examined by collecting cyclic voltammetry (CV) curves. The electrochromic color range characterized by transmittance at 633 nm was in situ recorded by time-resolved optical measurements. The obtained CV curves and corresponding in situ transmittance variation were plotted in **Figure 2**a,b, respectively, exemplified with those of the 1st and 50th cycle. The solid lines in Figure 2a depict the typical CV curves of the electrode in aqueous solutions of HCl, NaCl, and $AlCl_3$, with equal concentrations of 1.0 M. The $W_{18}O_{49}$ nanowire film in electrolyte solutions of NaCl only gave a pair of rather weak and broad redox peaks, among which potential for one reduction peak was even close to −1.2 V, indicating that the Na^+ ion was too large to be inserted into the $W_{18}O_{49}$ lattice framework. In clear contrast, profiles for $W_{18}O_{49}$ nanowires film in aqueous HCl and $AlCl_3$ exhibited excellent pesudocapacitive behavior and possessed much richer structure, featuring

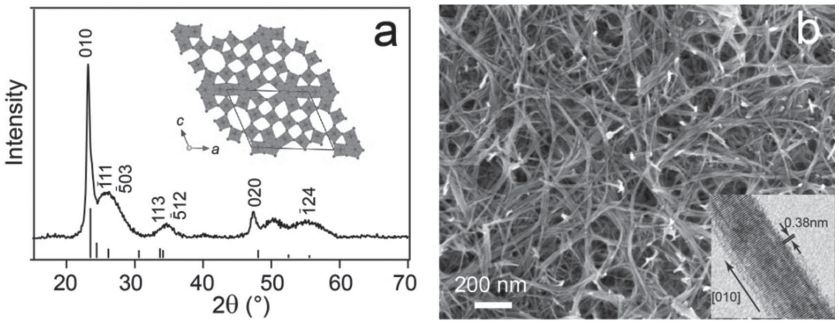

Figure 1. a) XRD pattern of the sample prepared from solvothermal reaction of WCl_6 in ethanol solution. The samples were scratched off from the substrate before characterizations to minimize the interference of FTO on substrate. All reflections could be perfectly fitted in a monoclinic cell (*P*2/*m*) of $W_{18}O_{49}$. Inset: [010] projection view of $W_{18}O_{49}$. b) Typical SEM image of the as-obtained sample manifesting a nanowire morphology. Inset: HRTEM image showing the nanowire were preferably grown along the [010] direction.

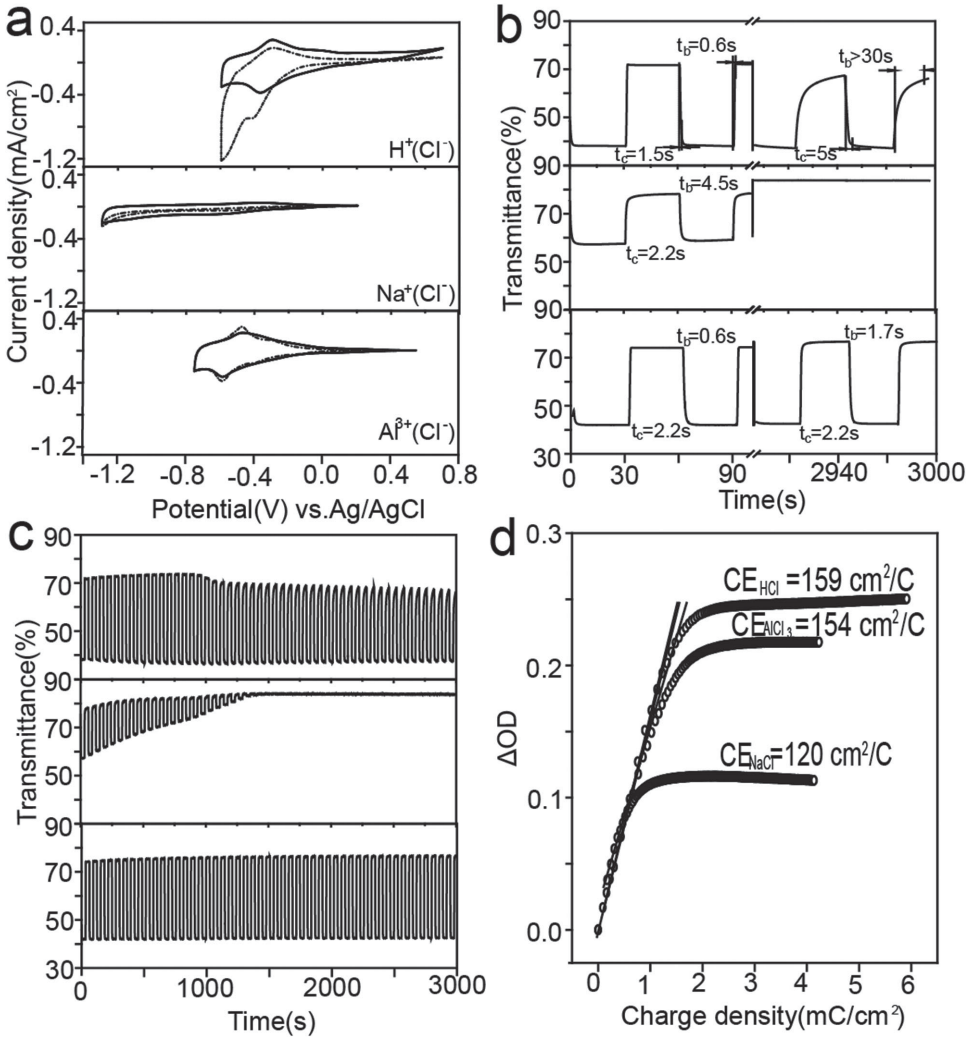

Figure 2. a) Solid lines: CV curves of the $W_{18}O_{49}$ nanowire film in 1.0 M aqueous solutions of HCl, NaCl, and $AlCl_3$, scan rate: 10 mV s^{-1}; broken lines: CV curves after 50 cycles of electrochromism test. b) In situ transmittance variation curves between colored and bleached state for $W_{18}O_{49}$ nanowires film in the three solutions. Solid and broken lines are for the 1st and 50th cycle, respectively. c) Full-range profiles of the transmittance change for the film electrode in the three solutions, showing good cycle stability for Al^{3+}. d) Plot of in situ OD variation as a function of charge density monitored at wavelength of 633 nm.

well-resolved redox peaks. Furthermore, the anodic and cathodic peak potential for the sample in $AlCl_3$ aqueous solution was located at –0.5 V and –0.55 V, only slightly negative compared to that for the sample in HCl aqueous solution, which suggests that the Al^{3+} insertion/extraction in the $W_{18}O_{49}$ lattice was also rather quick, comparable to the behavior of H^+. Accordingly, the switching time for Al^{3+} and H^+ was much narrower than that for Na^+, especially in the coloring process. The switching time is generally characterized as the required period for 90% of the optical change between the steady bleached and colored states. The time for bleaching and coloring of $W_{18}O_{49}$ nanowires electrode in $AlCl_3$ was about 2.2 s and 0.6 s, nearly as speedy as that for HCl, bleaching in 0.6 s and coloring in 1.5 s, contrasting obviously with the slow response for NaCl, 4.5 s and 2.2 s, respectively. In addition, the optical modulation in $AlCl_3$ and HCl was as large as 30%, while the electrode in NaCl solution only obtained a much narrowed modulation below 20%.

Al^{3+} not only gave comparable electrochemical behavior properties as H^+ in the first cycle, but also largely outperforms H^+ in cycle stability. The CV curves of the 50th cycle were given as broken lines in Figure 2a. Na^+ showed a great capacitive loss after 50 switching cycles with nearly complete disappearance of the loop feature in CV curve, indicating that Na^+ intercalation into $W_{18}O_{49}$ framework was extremely low after repetitive cycles, which would unavoidably deteriorate electrochromic properties. Consequently, after cycles the electrode was kept at bleached state and could not reverse back to the colored state via ion intercalation (Figure 2b). Such progressive deterioration also happens to H^+, consistent with previous studies.[27] The CV curves for H^+ became asymmetric with the occurrence of additional redox peaks at –0.41 and –0.59 V, suggesting poor

reversibility of the H^+ intercalation–deintercalation process, which may result from the trapping of charge due to irreversible chemical reactions between tungsten oxide matrix and the inserted H^+ ions during the cycles. The electrochromic performance accordingly became much inferior after 50 cycles. The switch time for coloring and bleaching significantly extended, from 1.5 to 5 s and 0.6 to >30 s, respectively. Furthermore, the modulation range progressively became smaller from about 30% to below 20%. In clear contrast, the CV profiles for Al^{3+} was almost unchanged even after the 50 cycles, demonstrating that the Al^{3+} intercalation–deintercalation process was highly reversible and the colored/switched states were stable. A close examination of the 50th cycle showed that the coloration/bleaching time for Al^{3+} remained short, 1.7/2.2 s, and the modulation range was also basically unchanged, remaining ≈30%. To the best of our knowledge, this is the first time that the excellent electrochromic stability has been achieved using Al^{3+} as insertion ion. The excellent electrochemical and electrochromic behavior is probably originated from the relative small radius size of Al^{3+} and the resultant easiness to be inserted into the electrode host and high stability of the Al^{3+}-intercalated phase. The improvement in cyclability and stability makes it possible for Al^{3+} ion to be applied to practical electrochromic devices.

Coloration efficiency (CE), an important parameter for electrochromic materials, is defined as the change in optical density (OD) per unit of inserted charge[28]

$$CE = \Delta OD/\Delta Q = log\,(T_b/T_c)/\Delta Q \quad (1)$$

where ΔQ refers to the inserted charge that yields the ΔOD change in the optical absorbance, T_b and T_c are the bleached and colored transmittance at a certain wavelength, respectively. The CE can be accordingly evaluated from the slope of the plots of ΔOD versus the charge density (Figure 2d). The calculated CE for Al^{3+} (154 $cm^2\ C^{-1}$) was almost the same as that for H^+ (159 $cm^2\ C^{-1}$), but notably higher than the value found for Na^+ (120 $cm^2\ C^{-1}$), which suggests that a small amount of injected charge in $AlCl_3$ solution can promotes large color change in $W_{18}O_{49}$ material. For a deeper understanding of Al^{3+}-insertion kinetics, the diffusion coefficient (D), which depicts the ion diffusion rate in $W_{18}O_{49}$ material, can be deduced based on the positive current peaks from a series of CV curves at different scan rates according to the Randles–Sevcik formula (Supporting Information). The D values obtained for H^+ and Al^{3+} were 5.29×10^{-10} $cm^2\ s^{-1}$ and 2.53×10^{-10} $cm^2\ s^{-1}$, respectively. The resulting diffusion coefficient for Al^{3+} was comparable to that for H^+, indicating superior insertion kinetics as H^+.

2.3. Electrochemical and Electrochromic Behavior in Nonaqueous Electrolyte

Aqueous electrolytes, however, generally suffer from narrow potential windows and consequently fast device degradation is a major problem for electrodes working in aqueous media.[29] Therefore, most practical electrochromic devices utilize lithium salt as electrolyte in nonaqueous solvent. To promote the understanding of the effect of Al^{3+} on the nonaqueous electrochromic process, we compared the electrochromic response of $W_{18}O_{49}$ nanowires under electrochemical insertion from one of the three different ions: Li^+, Na^+, and Al^{3+} in organic polycarbonate (PC) solvent using ClO_4^- as counter ion under ambient conditions. The same characterization procedures as those in aqueous electrolyte were employed, through cyclic electrochemical and in situ electrochromic test; the behaviors of $W_{18}O_{49}$ electrode in organic electrolyte were examined. As the bleaching or coloring in organic electrolyte was relatively slow, each cycle was extended to 50 s. The total period was controlled equal as that for study in aqueous electrolytes at 3000 s, and therefore the number of cycle was 30. The solid lines in **Figure 3**a shows CV curves of the 1st cycle for inserting or extracting Li^+, Na^+, and Al^{3+} into/from $W_{18}O_{49}$ nanowires. The anodic potentials for Li^+, Na^+, and Al^{3+} were −1.0, −1.3, and −0.1 V, with the one for Al^{3+} significantly shifted to the positive direction, implying that Al^{3+} insertion/extraction process in organic PC phase is kinetically much faster compared with Li^+ and Na^+. The much negative value for Na^+ should be in relation with its large ion radius. The fast kinetics of Al^{3+} ion leads to a significant enhancement in electrochromic performance both in switching time and in color contrast. The $W_{18}O_{49}$ nanowire films in Al^{3+} electrolyte showed short switching time of 5.8 s for the bleaching step and 4.1 s for the reverse process, while the time period in Li^+ and Na^+ showed a much slower temporal response with bleaching/coloring time of 11.3/4.2 s and 8.3/2.8 s, respectively (Figure 3b). The color contrast of Al^{3+} also benefits from the fast kinetics with a higher modulation range up to about 32%, whereas Li^+ and Na^+ only reached a value of ≈20% and 10%, respectively (Figure 3c).

Regarding cyclability and stability, all the three cases delivered good behaviors as expected without the occurrence of asymmetric peaks in H^+ or obvious loss of capacitive behavior in Na^+ electrolyte. It is noteworthy that along with the progression of electrochemical cycles the high-coloration contrast was well maintained only in Al^{3+} case, still having ≈30% even after 30 repeated cycles, which further confirmed that the superior cycling stability of Al^{3+}. The advantage of utilizing Al^{3+} as electrolyte in both aqueous and nonaqueous electrochemical reactions was obvious, which could bring long-desired characteristics such as fast switching and excellent cyclic stability of electrochromic performance.

Meantime, the study of CE and ion diffusion rate provided addition evidence that Al^{3+} could deliver superior insertion kinetics. The CE values of $W_{18}O_{49}$ nanowires film in Al^{3+} electrolyte (68 $cm^2\ C^{-1}$) was slightly lower than that in Li^+ electrolyte (89 $cm^2\ C^{-1}$) but higher than that in Na^+ electrolyte (44 $cm^2\ C^{-1}$). The diffusion coefficients for Li^+, Na^+, and Al^{3+} were calculated to be 2.18×10^{-10}, 7.12×10^{-11}, and 1.59×10^{-10} $cm^2\ s^{-1}$ for the electrochromic process, respectively (Supporting Information). Apparently, the ion diffusion rate of Al^{3+} was comparable with that for Li^+ but significantly higher than that for Na^+. The behavior parameters were summarized in **Table 1**, demonstrating that the goal of fast response, high-contrast and high stability could all be achieved utilizing Al^{3+} as the electrolyte, in both aqueous and nonaqueous solutions.

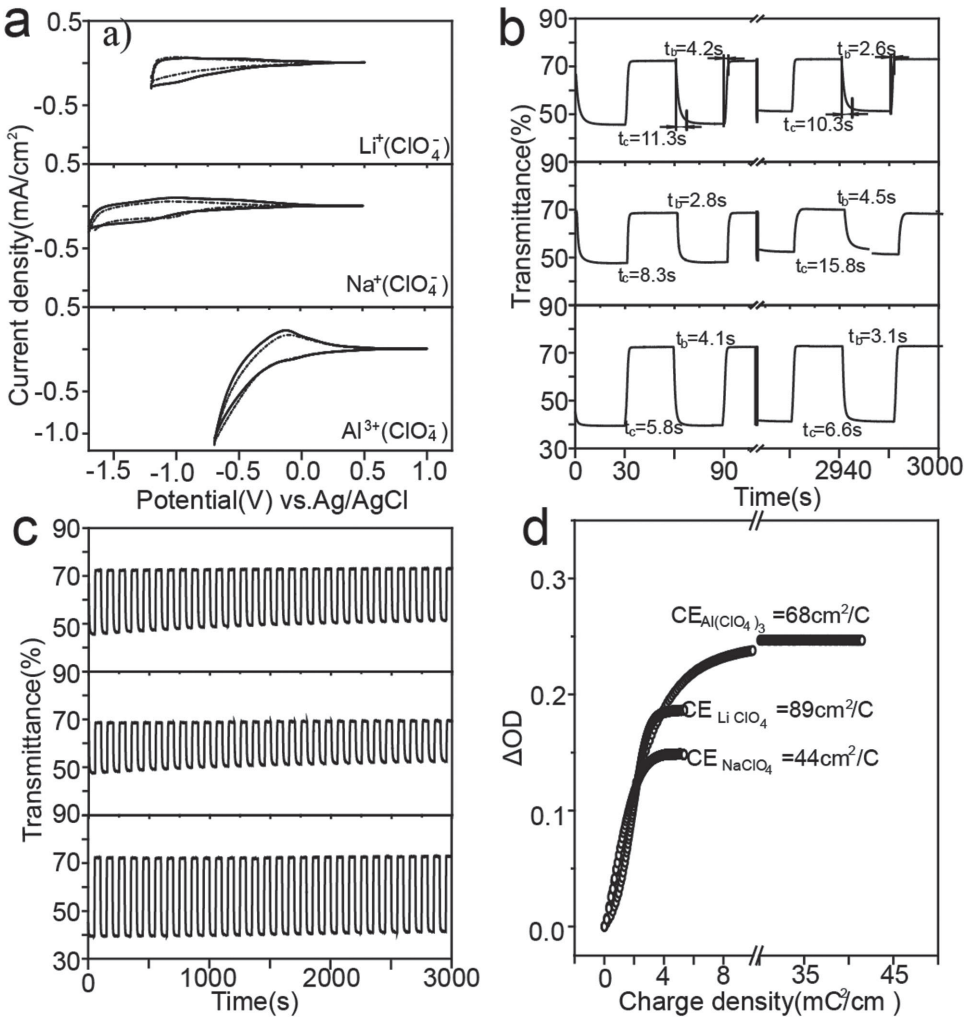

Figure 3. a) CV curves (solid: the 1st cycle, broken: the 30th cycle) of the $W_{18}O_{49}$ nanowires film at a scan rate of 10 mV s^{-1} in 1.0 M PC-$Al(ClO_4)_3$, PC-$LiClO_4$, PC-$NaClO_4$. b) In situ transmittance variation curve between colored and bleached state for $W_{18}O_{49}$ nanowires film in 1.0 M PC-$Al(ClO_4)_3$, PC-$LiClO_4$, and PC-$NaClO_4$. Solid and broken lines are for the 1st and 30th cycle, respectively. c) Full plot of the in situ transmittance variation in the three nonaqueous solutions, a total of 30 cycles. d) In situ OD variation as a function of charge density monitored at wavelength of 633 nm in PC-$LiClO_4$, PC-$NaClO_4$, PC-$Al(ClO_4)_3$.

2.4. Spectral Study with Al^{3+}-Intercalation

The electrochromic phenomena in tungsten oxide upon Al^{3+} intercalation can be described by the following equation:

$$W_{18}O_{49} + 3xe^- + xAl^{3+} \leftrightarrow AlxW_{18}O_{49} \quad (2)$$

An attractive aspect of using Al^{3+} as insertion ions in electrochromic applications was that the electrochromic cycling stability was significantly improved in nanostructured metal oxide

Table 1. A summary of electrochromic behavior of the electrodes.

	Aqueous				Nonaqueous				
	T_b [s] $1^{st}\rightarrow50^{th}$	T_c [s] $1^{st}\rightarrow50^{th}$	OD $1^{st}\rightarrow50^{th}$	CE [cm^2 C^{-1}]	CE [cm^2 C^{-1}]	OD $1^{st}\rightarrow50^{th}$	T_c [s] $1^{st}\rightarrow50^{th}$	T_b [s] $1^{st}\rightarrow50^{th}$	
H^+	0.6→>>30	1.5→5	30%→20%	159					
					89	20%→15%	4.2→2.6	11.3→10.3	Li^+
Na^+	4.5→NA*	2.2→NA*	20%→0	120	44	10%→8%	2.8→4.5	8.3→15.8	Na^+
Al^{3+}	0.6→1.7	2.2→2.2	30%→30%	154	68	30%→30%	4.1→3.1	5.8→6.6	Al^{3+}

The T_b and T_c for Na^+ after 50 repeated cycles were not available (NA) because capacitive behavior was almost completely lost after 50^{th} cycles.

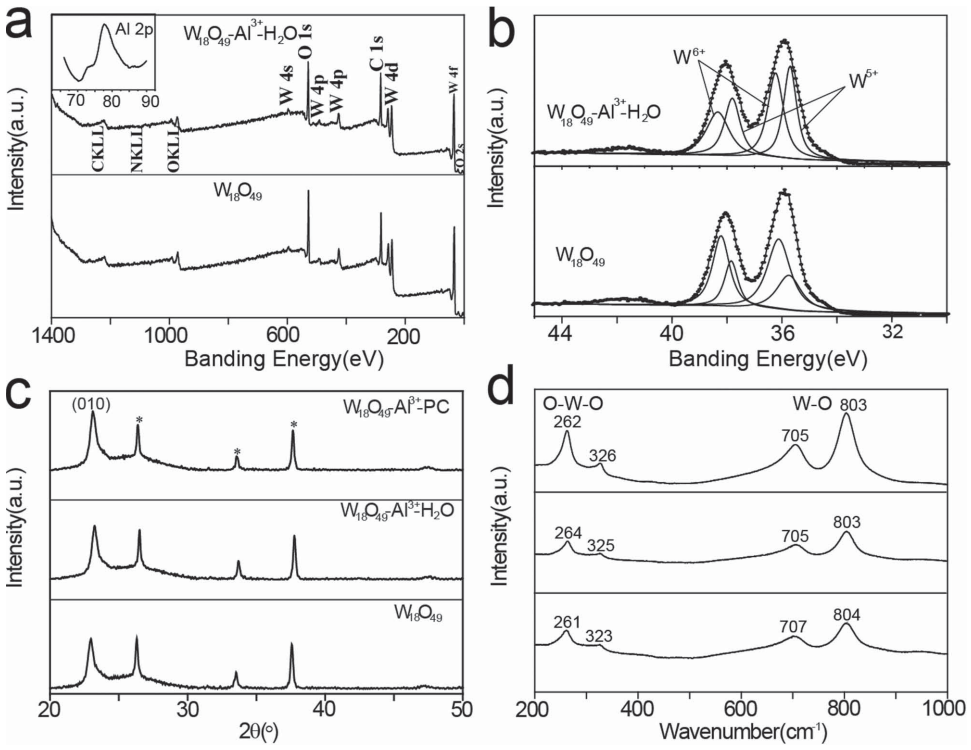

Figure 4. a) Full XPS profiles for original $W_{18}O_{49}$ nanowire film and the film after Al ion intercalation. Inset: Al2p XPS spectrum indicating the successful insertion of Al^{3+} ions. b) XPS spectrum of W4f core level peaks showing peaks corresponding to W^{6+} and W^{5+}, through which the ratio of W^{5+}/W^{6+} was evaluated. After Al^{3+} intercalation, the ratio increased to 0.86 from 0.57 for the original sample. c, d) XRD patterns and Raman spectra for original $W_{18}O_{49}$ nanowire film and the films after XPS spectrum of W4f core level peaks.

hosts compared with the conventional monovalent insertion ions, while keeping other favorable electrochromic parameters such as fast switching, high contrast. We believe the high cyclic stability benefits from the unique insertion mechanism of Al^{3+}. The insertion of Al^{3+} was verified by X-ray photoelectron spectroscopy (XPS) characterizations. XPS survey spectrum of the $W_{18}O_{49}$ nanowire electrodes before and after Al^{3+} intercalation in **Figure 4**a indicated the sample after intercalation contained element Al in addition to W and O. A close scan of Al^{3+} in the inset detected a broad, asymmetric peak appeared at 76.4 eV, corresponding to the Al 2p peak of Al^{3+},[30] confirming that Al was intercalated into the $W_{18}O_{49}$ framework in Al^{3+} form. A direct consequence of Al^{3+} intercalation was that the part of W^{6+} in $W_{18}O_{49}$ was reduced chemically, resulting an increase in ration of W^{5+}/W^{6+}, which was evidenced by XPS measurements,[31] increasing from 0.57 for original sample to 0.86 after Al^{3+} insertion (Figure 4b). Meantime, XRD measurement showed that Al^{3+}-intercalation did not bring significant phase change, without the detection of any impurities (Figure 4c). No obvious diffraction broadening was observed, suggesting that the crystallinity was also well remained. Noteworthy, accompanying the insertion of Al^{3+}, the peak position of (010) shifted to high-angle region, suggesting the cell dimension along the growth direction, *b*-axis, was contracted instead of expansion. The intercalation of guest, for example, monovalent ions H^+, Li^+, or Na^+, traditionally brought expansion, which would generally degrade the host materials and limits the life time of electrochromic devices.[32] The abnormal trend may result from the strong electrostatic interactions between Al^{3+} and the intercalation framework. The contraction along the *b* axis with the intercalation of Al^{3+} ion was also evidenced by the fact that the spacing of (010) plane of a $W_{18}O_{49}$ nanowires lattice in HRTEM images reduced from 0.38 nm to 0.36 nm (in the aqueous electrolyte) and 0.35 nm (in the nonaqueous electrolyte) after Al^{3+} insertion, respectively (Supporting Information). The microstructure information of the samples was obtained through Raman study with the Raman spectra before and after Al^{3+} intercalation depicted in Figure 4d. The W–O stretching modes at 706 cm^{-1} and 804 cm^{-1} in the high wavenumbers region and the O–W–O bending modes at 260 and 323 cm^{-1} in the low wavenumbers region were both observed, in good agreement with the previously reported characteristics modes of $W_{18}O_{49}$.[33] After Al^{3+} insertion, the W–O stretching modes red shifted to 705 and 803 cm^{-1}, and the O–W–O bending modes blue shifted to 262 and 325 cm^{-1}, implying that the W–O bond in WO_6 octahedron became weakened and the O–W–O in the WO_6 octahedron became strengthened. The WO_6 octahedra were resultantly compressed, which is consistent with the XRD observation of contraction along the *b*-axis. Therefore, differing from the structure degradation by repeated guest intercalation/deintercalation, the Al^{3+} insertion brought structure contraction along the *b*-axis while remaining the crystallinity, which on some degree stabilized the crystal structure and consequently produced much enhanced cyclability.

3. Conclusion

In summary, breaking the traditional concept of using monovalent ions such as H^+, Li^+, Na^+ as the insert ions in EC applications, it is the first time that using the trivalent Al^{3+} as insertion ion to obtain fast switching, high contrast, and highly stable electrochromic behavior. The new application of Al^{3+} in electrochromism makes it possible to overcome the existing problems encountered for the conventional insertion ions such as strong tendency to destroy the host material, high cost, and hard handling, while still exhibits wide optical modulation, fast color-switching speed, high CE and good cyclic stability. We believe electrochromic research would benefit from the new, low-cost insertion ion to fabricate more stable, more economical electrochromic devices.

4. Experimental Section

Preparation of $W_{18}O_{49}$ Nanowire Film on FTO glass: The details of the growth of $W_{18}O_{49}$ nanowire films have been described before.[24] In a typical synthesis, 0.099 g of WCl_6 was dissolved into 30 mL of absolute ethanol, which was transferred to a Teflon-lined stainless steel autoclave, holding a vertically oriented FTO glass substrate. The autoclave was then sealed and maintained at 180 °C for 12 h. After reactions, the substrate was taken out and rinsed thoroughly with distilled water and absolute ethanol before being dried at 60 °C for 12 h. The as-prepared product was further annealed in argon gas at 200 °C for 1 h, which yielded the $W_{18}O_{49}$ nanowires structure on FTO.

Characterization: Field emission scanning electron microscopy (FE-SEM) analysis was performed on a FEI Quanta 400 FEG field emission scanning electron microscope. TEM images were obtained employing JEOL 2010 with beam energy of 100 kV. XRD patterns of the prepared samples were recorded on a Bruker AXS D8 Advance X-ray diffractometer with a Cu Ka radiation target (40 V, 40 A). Raman spectra were collected with a LabRAM HR Evolution instrument using red (633 nm) lasers.

Electrochemical and Optical Measurement: UV–vis experiments were made in transmission geometry on a UV–vis spectrophotometer (V660, JASCO) over a wavelength range of 200–900 nm. Electrochemical measurements were carried out on an electrochemical workstation (Dual Electrochemical Workstation ZIVE BP2) using a conventional three-electrode test cell. A platinum wire was used as counter electrode and a KCl saturated Ag/AgCl as reference electrode.

Supporting Information

Supporting Information is available from the Wiley Online Library or from the author.

Acknowledgements

This work was supported by the National Natural Science Foundation of China (51372266), the Natural Science Foundation of Jiangsu Province (BK20130348), and Suzhou Industrial Science and Technology Programm (ZXG201426). F.X.G. acknowledges the support of the National Natural Science Foundation of China (51402204), Thousand Young Talents Program, and Jiangsu Specially-Appointed Professor Program.

Received: June 28, 2015
Revised: July 22, 2015
Published online: August 13, 2015

[1] J. Matsui, R. Kikuchi, T. Miyashita, *J. Am. Chem. Soc.* **2013**, *136*, 842.
[2] H. Demiryont, D. Moorehead, *Sol. Energy Mater. Sol. Cells* **2009**, *93*, 2075.
[3] R. J. Mortimer, A. L. Dyer, J. R. Reynolds, *Displays* **2006**, *27*, 2.
[4] G. A. Niklasson, C. G. J. Granqvist, *Mater. Chem.* **2007**, *17*, 127.
[5] C. G. Granqvist, *Sol. Energy Mater. Sol. Cells* **2012**, *99*, 1.
[6] J. Huang, *Pure Appl. Chem.* **2006**, *78*, 15.
[7] M. Wagemaker, A. P. M. Kentgens, F. M. Mulder, *Nature* **2002**, *418*, 397.
[8] S. J. Yoo, J. W. Lim, Y. E. Sung, Y. H. Jung, H. G. Choi, D. K. Kim, *Appl. Phys. Lett.* **2007**, *90*, 173126.
[9] T. Brezesinski, D. Fattakhova Rohlfing, S. Sallard, M. Antonietti, B. M. Smarsly, *Small* **2006**, *2*, 1203.
[10] J. Z. Chen, W. Y. Ko, Y. C. Yen, P. H. Chen, K. J. Lin, *ACS Nano* **2012**, *6*, 6633.
[11] F. Cheng, J. Liang, Z. Tao, J. Chen, *Adv. Mater.* **2011**, *23*, 1695.
[12] W. Wang, B. Jiang, W. Xiong, H. Sun, Z. Lin, L. Hu, J. Tu, J. Hou, H. Zhu, S. Jiao, *Sci. Rep.* **2013**, *3*, 3383.
[13] F. D. Dini, E. Decker, J. Masetti, *Appl. Electrochem.* **1996**, *26*, 647.
[14] H. Tokudome, M. Miyauchi, *Angew. Chem. Int. Ed.* **2005**, *44*, 1974.
[15] R. Kirchgeorg, S. Berger, P. Schmuki, *Chem. Commun.* **2011**, *47*, 1000.
[16] M. R. J. Scherer, U. Steiner, *Nano Lett.* **2012**, *13*, 3005.
[17] C. Xiong, A. E. Aliev, B. Gnade, K. J. Balkus, *ACS Nano* **2008**, *2*, 293.
[18] G. F. Cai, J. P. Tu, D. Zhou, X. L. Wang, C. D. Gu, *Sol. Energy Mater. Sol. Cells* **2014**, *124*, 103.
[19] S. Adhikari, D. Sarkar, *Electrochim. Acta.* **2014**, *138*, 115.
[20] C. Yan, W. Kang, J. Wang, M. Cui, X. Wang, C. Y. Foo, K. J. Chee, P. S. Lee, *ACS Nano* **2013**, *8*, 316.
[21] L. Liu, M. Layani, S. Yellinek, A. Kamyshny, H. Ling, P. S. Lee, S. Magdassi, D. Mandler, *J. Mater. Chem. A* **2014**, *2*, 16224.
[22] S. Cong, Y. Tian, Q. Li, Z. Zhao, F. Geng, *Adv. Mater.* **2014**, *26*, 4260.
[23] B. J. W. Liu, J. Zheng, J. L. Wang, J. Xu, H. H. Li, S. H. Yu, *Nano Lett.* **2013**, *13*, 3589.
[24] Y. Tian, S. Cong, W. Su, H. Chen, Q. Li, F. Geng, Z. Zhao, *Nano Lett.* **2014**, *14*, 2150.
[25] M. S. Zhu, W. J. Meng, Y. Huang, Y. Huang, C. Y. Zhi, *ACS Appl. Mater. Interfaces* **2014**, *6*, 18901.
[26] G. Xi, S. Ouyang, P. Li, J. Ye, Q. Ma, N. Su, H. Bai, C. Wang, *Angew. Chem. Int. Ed.* **2012**, *51*, 2395.
[27] S. H. Lee, R. Deshpande, P. A. Parilla, K. M. Jones, B. To, A. H. Mahan, A. C. Dillon, *Adv. Mater.* **2006**, *18*, 763.
[28] S. H. Lee, H. M. Cheong, C. E. Tracy, A. Mascarenhas, A. W. Czanderna, S. K. Deb, *Appl. Phys. Lett.* **1999**, *75*, 1541.
[29] Y. S. Lin, Y. C. Chen, P. S. Shie, *Sol. Energy Mater. Sol. Cells* **2014**, *122*, 59.
[30] A. P. Huang, G. J. Wang, S. L. Xu, M. K. Zhu, G. H. Li, B. Wang, H. Yan, *Mater. Sci. Eng. B* **2004**, *107*, 161.
[31] S. Jeon, K. Yong, *J. Mater. Res.* **2008**, *23*, 1320.
[32] H. Wu, G. Zheng, N. Liu, T. J. Carney, Y. Yang, Y. Cui, *Nano Lett.* **2012**, *12*, 904.
[33] D. Y. Lu, J. Chen, S. Z. Deng, N. S. Xu, W. H. Zhang, *J. Mater. Res.* **2008**, *23*, 402.